Metal Semiconductor Field-Effect Transistor with MoS_2/Conducting NiO_x van der Waals Schottky Interface for Intrinsic High Mobility and Photoswitching Speed

Hee Sung Lee,[†] Seung Su Baik,[‡] Kimoon Lee,[§] Sung-Wook Min,[†] Pyo Jin Jeon,[†] Jin Sung Kim,[†] Kyujin Choi,[†] Hyoung Joon Choi,[‡] Jae Hoon Kim,[†] and Seongil Im*,[†]

[†]Institute of Physics and Applied Physics, Yonsei University, Seoul 120-749, Korea, [‡]Center for Computational Studies of Advanced Electronic Material Properties, Yonsei University, Seoul 120-749, Korea, and [§]Department of Physics, Kunsan National University, 558 daehak-ro, Gunsan, Jeonbuk 573-701, Korea

ABSTRACT Molybdenum disulfide (MoS_2) nanosheet, one of two-dimensional (2D) semiconductors, has recently been regarded as a promising material to break through the limit of present semiconductors. With an apparent energy band gap, it certainly provides a high carrier mobility, superior subthreshold swing, and ON/OFF ratio in field-effect transistors (FETs). However, its potential in carrier mobility has still been depreciated since the field-effect mobilities have only been measured from metal−insulator−semiconductor (MIS) FETs, where the transport behavior of conducting carriers located at the insulator/MoS_2 interface is unavoidably interfered by the interface traps and gate voltage. Moreover, thin MoS_2 MISFETs have always shown large hysteresis with unpredictable negative threshold voltages. Here, we for the first time report MoS_2-based metal semiconductor field-effect transistors (MESFETs) using NiO_x Schottky electrode which makes van der Waals interface with MoS_2. We thus expect that the maximum mobilities or carrier transport behavior of the Schottky devices may hardly be interfered by interface traps or an on-state gate field. Our MESFETs with a few and ~10 layer MoS_2 demonstrate intrinsic-like high mobilities of 500−1200 $cm^2/(V\,s)$ at a certain low threshold voltage between −1 and −2 V without much hysteresis. Moreover, they work as a high speed and highly sensitive phototransistor with 2 ms switching and ~5000 A/W, respectively, supporting their high intrinsic mobility results.

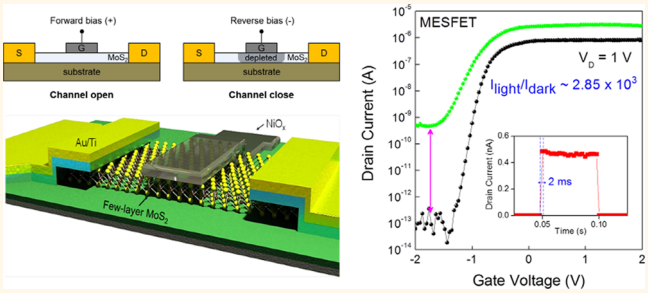

KEYWORDS: 2D nanosheet MoS_2 · NiO_x · MESFET · Hall measurement · Schottky junction · van der Waals interface

Until recent years, molybdenum disulfide (MoS_2) nanosheet among many two-dimensional (2D) transition metal dichalcogenide semiconductors[1−22] has been regarded as one of the most promising materials to break through the limit of present semiconductors.[3−10] With an apparent energy band gap, of which the range is 1.2−1.8 eV depending on the MoS_2 thickness,[2,7] it certainly provides a high carrier mobility, superior subthreshold swing (SS), and ON/OFF current ratio in metal insulator semiconductor field-effect transistors (MISFETs).[2−11] The highest mobility has been mostly achieved from few layer MoS_2 MISFETs with a top-gate high-k dielectric layer.[3−5,7,8,10,11] However, their field-effect mobility is in a wide range from 10 to 1000 $cm^2/(V\,s)$ and their threshold voltages are not reproducibly consistent, either, in reports because those values should be seriously dependent upon the dielectric/MoS_2 interface and bulk trap states in a MISFET where in particular the mobility is influenced by the gate voltage as well.[23,24] As a result, the potential or intrinsic carrier mobility of MoS_2 has not been properly appreciated yet since the field-effect mobilities have mostly been measured from MISFET structures,[25,26] where the interface/bulk traps and gate

* Address correspondence to semicon@yonsei.ac.kr.

Received for review May 8, 2015 and accepted July 14, 2015.

Published online July 14, 2015
10.1021/acsnano.5b02785

voltage unavoidably interfered with the transport behavior of conducting carriers located at the insulator/MoS_2 interface.[23,24] Moreover, the top-gate high mobility MoS_2 MISFETs have often shown unpredictable and large negative threshold voltages.[8,11,27,28]

To resolve such issues in MoS_2 FETs, we report, for the first time, metal semiconductor field-effect transistors (MESFETs)[29,30] with MoS_2–NiO_x van der Waals Schottky junction interface, where the maximum mobilities or carrier transport behavior of the Schottky devices may hardly be interfered with by interface traps or an on-state gate field.[30,31] Our MESFETs with a few and ~10 layer MoS_2 demonstrate high mobilities of 500–1200 $cm^2/(V\ s)$ approaching their intrinsic room temperature mobilities at a certain low threshold voltage between −1 and −2 V with little hysteresis. Moreover, they work as a high speed and highly sensitive phototransistor with 2 ms switching and ~5000 A/W, respectively, supporting their high intrinsic mobility results.

RESULTS AND DISCUSSION

Figure 1a displays the top view optical microscopy image of the MESFET with 10-layer MoS_2 channel contacting 150 nm-thick thermally evaporated NiO_x gate (G) on 285 nm-thick SiO_2/p^+-Si substrate. According to the image, the MoS_2 flake shape is a little oblique to the source (S)-to-drain (D). NiO_x is known to have quite a deep work function of more than 5.1–5.2 eV as a Ni-rich semitransparent conducting oxide ($x \sim 0.9$).[32,33] For a S/D ohmic contact, we utilized an Au/Ti bilayer, so that Ti might contact our MoS_2 nanosheet, as shown in the schematic three-dimensional (3-D) view of our MESFET device of Figure 1c. The channel thickness of our 10-layer MoS_2 on 285 nm-thick SiO_2/p^+-Si was confirmed by atomic force microscope (AFM) scan in Figure 1b and its inset topological 3-D image.

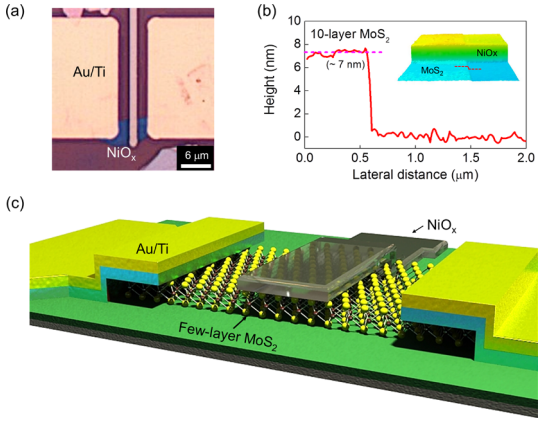

Figure 1. (a) Top views of our MESFET with 10-layer MoS_2, NiO_x top-gate, and Au/Ti source/drain in an optical microscopy. (b) AFM topography results from 10-layer thin MoS_2 channel in MESFET (thickness was measured to be ~7 nm). (c) Schematic 3D view of MoS_2-based MESFET with 6 μm-long channel, 3 μm-long NiO_x gate, and S/D region in contact with Ti.

(Other optical microscopies of thick MoS_2 nanosheets are also displayed in Supporting Information Figure S1.)

To achieve any typical operation of MESFET, the following two conditions should be met. First, Schottky barrier should be clearly formed between the gate and channel semiconductor nanosheet, so that the G-to-S or G-to-D Schottky diode operates as a rectifier. According to the current–voltage (I–V) characteristics from the 10- and 60-layer MoS_2/NiO_x diode junction in Figure 2a, the 40 nm-thick MoS_2 (with 60-layer) was not able to properly form any good Schottky junction with NiO_x showing very small ON/OFF ratio of less than 10. On the other hand, 10-layer MoS_2 sheets appear to form good Schottky barriers with respect to NiO_x, showing 2.49 as an ideality factor. It is also recognized that the reverse leakage current becomes larger with the sheet thickness, indicating that some lowering of physical barrier takes place with a thick MoS_2. The Schottky barrier lowering is certainly related to the thickness-induced band gap reduction in MoS_2; the conduction band edge of MoS_2 might decrease with the thickness increase as its bandgap does decrease.[2,7] (Schematic illustrations and Schottky equations in Supporting Information Figures S2 and S3 help understanding these phenomenon.)

Second, the MESFET should turn on before the Schottky diode starts to operate, otherwise drain current (I_D) would be consumed by or leaked to the gate (joining the G-to-S leakage current, I_{GS}). As a matter of fact, we also fabricated Schottky pure metal (Pd and Pt)-driven MESFETs which did not work as an FET, although they operated well as a Schottky diode, because such deep work function metal gate device could not meet the second condition. (See Supporting Information Figure S4a,b.) It is interesting to note that unlike such cases of pure metal Schottky gate device, conducting NiO_x Schottky gate device operated very well as a MESFET. We suppose that this difference comes from a unique interface between thermally evaporated NiO_x and MoS_2, which would be much different from that between pure metal/MoS_2. In general, the pure metal contaminates the surface of MoS_2 due to an intimate chemical binding between metal and MoS_2 (Supporting Information Figure S4b),[34] while NiO_x would make only van der Waals interface[14–16,35,36] to MoS_2 so as not to cause gate leakage during FET operation. Our density-functional-theory calculations show that the NiO_x/MoS_2 interface has a large NiO_x–MoS_2 distance of 3.31 Å with no significant influence on the electric structure of MoS_2, while Ti/MoS_2 and Au/MoS_2 interfaces have Ti–MoS_2 and Au–MoS_2 distances of 1.60 and 2.60 Å, respectively, perturbing greatly the electronic structure of MoS_2.

Corresponding to the results of Figure 2a, the drain current–gate voltage (I_D–V_{GS}) transfer characteristics are, respectively, achieved from the two MoS_2

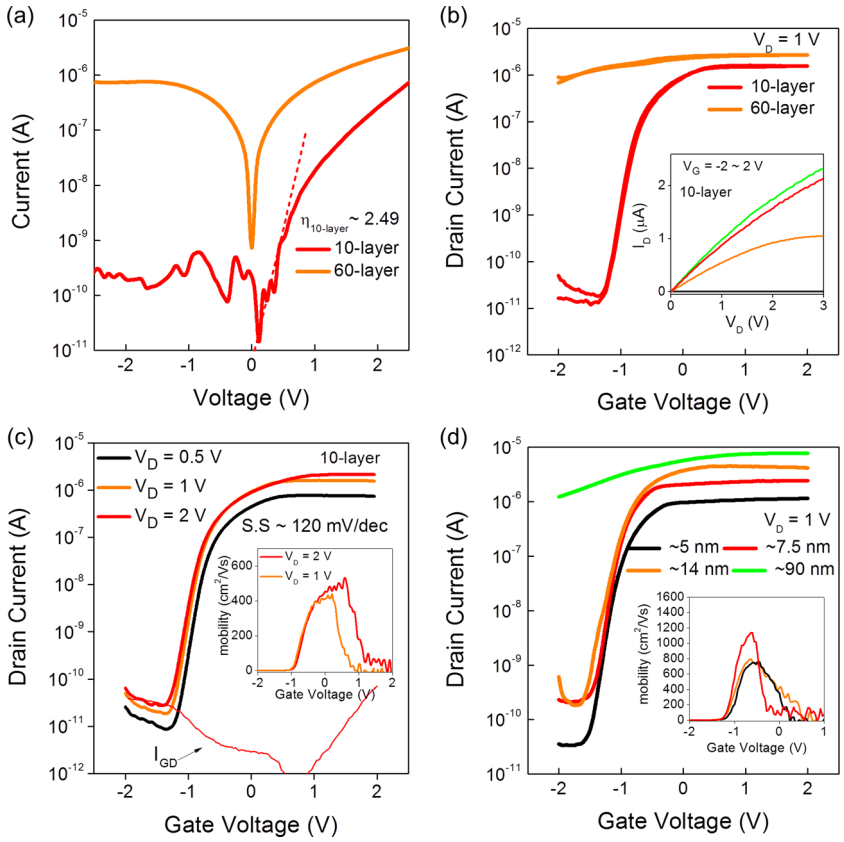

Figure 2. (a) $I-V$ characteristics of Schottky diodes with 10- and 60-layer MoS_2. Diode behavior was clearly observed from 10-layer MoS_2 with NiO_x and Au/Ti electrodes, while the Schottky behavior of the thick MoS_2 diode appears very weak along with large reverse current. (b) I_D-V_G transfer curves of our MESFETs with 10- and 60-layer MoS_2 obtained at a V_D of 1 V; the device with 60-layer thick MoS_2 operates as an almost simple resistor. The inset shows output curves of 10-layer MoS_2 MESFET. (c) I_D-V_G transfer and $I_{GD}-V_G$ gate leakage curves of the MESFET with 10-layer MoS_2, as measured with V_D increase; SS was ~120 mV/dec and inset curves show the saturation mobility plots. (d) Transfer curves of MESFETs with several MoS_2 thicknesses obtained at a V_D of 1 V; the device with 90 nm-thick MoS_2 operates as an almost simple resistor. The inset shows saturation mobility plots of 5 nm (7-layer), 7.5 nm (11-layer), and 14 nm (20-layer)-thick MoS_2 MESFETs.

nanosheet-based MESFETs as shown in Figure 2b, where MESFET operations are nicely observed from 10-layer MoS_2 devices as induced by the V_{GS}-dependent charge-depletion-modulation (which is not just to the thickness direction but also to in-plane direction).[37] According to the transfer curve of 10-layer MoS_2 MESFET achieved at a drain voltage (V_{DS}) of 1 V, its ON-current I_D appeared to be 1.6 μA along with ON/OFF ratio, OFF current, and SS properties of ~10^5, ~30 pA, and 120 mV/dec, respectively. Inset output curves of Figure 2b display that our 10-layer MoS_2 MESFET does not show perfect linear but somewhat saturation behavior as V_{DS} increases. The saturation I_D behavior probably originates from the fact that easy pinch-off is possible in MESFET with thin MoS_2 unlike MISFET with the same MoS_2 as we compare both FETs in later discussion. On the one hand, the 60-layer MoS_2 MESFET displays a resistor type behavior in Figure 2b, where its I_D appears almost independent of V_{GS} due to the thick MoS_2 channel. This resistor type behavior is understandable, since the thick MoS_2 induces only a little Schottky barrier which would hardly cause any sufficient channel depletion even under quite a large negative gate bias. On the basis of above results, it is regarded that a larger Schottky barrier induces more outstanding SS and ON/OFF (charge conduction/depletion) switching performance along with the sheet thickness.

One of the most important is probably how to determine the mobility (μ) of the 10-layer MoS_2 MESFET. According to the output curves, we want to use the saturation regime method for the mobility estimation as more general method; we can calculate the channel mobilities using transconductance (g_m) and the following equations,[30,38,39] since we have g_m plots depending on V_{DS}. (See Supporting Information Figure S5, for g_m plots.)

$$g_m = \frac{\partial I_D}{\partial V_G} = \frac{qN_d\mu tW}{L}$$

So, the maximum channel mobility can be calculated as follows,

$$\mu = \frac{Lg_{Max}}{qN_d tW}$$

where g_{Max} is a maximum value of g_m plot as a function of V_{GS}. N_d is carrier density as number per cm^3; q is an

electronic charge; and t, W, and L are the thickness, width, and length of the channel, respectively. Now, the most wanted information to determine the mobility is the electron carrier density, n, or unintentional doping concentration, N_d, according to above equations. N_d is reported to be in a range from $\sim 5 \times 10^{15}$ to 5×10^{16} cm^{-3} in general MoS_2 bulk crystals;[9,40−42] however, we here estimated the values of our own MoS_2 sheets by using two methods: the Padovani−Stratton parameter method[34,43] on 10-layer MoS_2 on SiO_2/p^+-Si (Supporting Information Figure S6 and Table S1) and the physical property measurement system (PPMS)-adopting AC current Hall measurements on 16 nm-thin (~23-layer) MoS_2 on glass.[44,45] We thus obtained respective n values of 1.42×10^{16} and 2.52×10^{16} cm^{-3}. (The electron density values of 10- and 23-layer MoS_2 are $\sim 1 \times 10^{10}$ and 4.1×10^{10} cm^{-2} in area density, which is about 2 orders of magnitude lower than that of gate charging state in MISFET.)[25,26] The electron density values are comparable to not only those reported for thick bulk MoS_2 in literature,[9,40−42] but also the previously reported value from Padovani−Stratton method for 12 nm-thin (~17-layer) MoS_2 on SiO_2/p^+-Si.[43] Nonetheless, we chose the number density of 2.52×10^{16} cm^{-3} as the most reliable room temperature N_d value, since it was more directly obtained by high magnetic field (maximum 10 T) Hall measurements. Figure 2c shows the transfer curves obtained from 10-layer MoS_2 MESFET at V_{DS} of 0.5, 1, and 2 V, while its inset displays maximum saturation mobility of the device, to be ~520 cm^2/(V s). The leakage current (I_{GD}) is also plotted in Figure 2c. The maximum I_{GD} is about 100 pA, which is quite smaller than I_D by more than 4 orders of magnitude, confirming the high quality of the NiO_x Schottky gate for the MoS_2 MESFET. A few other similarly thick MoS_2 MESFETs were fabricated to confirm this result of 10-layer MoS_2 MESFET. According to the respective transfer curves and saturation mobilities in Figure 2d and inset plots, 5 nm (7-layer), 7.5 nm (11-layer), and 14 nm (20-layer)-thick MoS_2 MESFETs display a range of high mobility between 760 and 1200 cm^2/(V s). (These are peak mobilities extracted by considering transconductance g_m plots, and the zero mobility beyond peak value in the plot is not much meaningful.) When the layer was too thick (90 nm), Schottky gate did not work. In this regard, our MESFET device with ~10 nm-thick MoS_2 channel demonstrates its intrinsic potential approaching to the intrinsic room temperature mobility of ~1000 cm^2/(V s). The mobility difference among all the MESFETs with 5−14 nm probably come from their respective S/D contact resistances which can be different depending on the contact area. From the transfer curves of Figure 2c,d, it is also worth to note that our all MESFETs have low operational or threshold voltages between −1 and −2 V with little gate hysteresis, since the FET gate opening in the present device is based on Schottky-driven operation on thin channels. The threshold voltage value is thus always predictable unlike the reported cases of MoS_2 MISFET,[8,11,27,28] to be marked as an important benefit of MESFET. All the electrical properties of our MESFET devices and MoS_2 thickness profiles are summarized in detail in Supporting Information Figure S7 and Table S2.

In the present study, we even implemented the temperature-dependent Hall measurements on 16 nm-thin MoS_2 on glass in the range of 200−300 K to confirm any reliability of our measurements on the electron number density or intrinsic doping density (n or N_d). Figure 3a shows an optical image of our 4-probe MoS_2 sample for Hall measurement, while AFM topography in Figure 3b indicates the sample thickness and surface morphology. To measure the Hall resistance (R_H) of our 16 nm-thin MoS_2 sample on glass substrate, we applied AC current of 0.4 Hz and 0.1 mA as input signal frequency and amplitude, respectively, under the magnetic field (H) sweep from −10 to 10 T. As shown in Figure 3c, linear dependence of R_H on H was clearly observed with various temperatures. (The inset plot of Figure 3d again shows a magnified view of linear R_H variation under H sweep at 300 K). Since the R_H can be determined to be,[44]

$$R_H = \frac{V_H}{I} = -\frac{H}{n_s q}$$

where, I is input current, V_H is Hall voltage, n_s is sheet carrier concentration (cm^{-2}), and q is electric charge, n_s can be estimated from the slope of R_H−H curve as below.

$$n_s = -\frac{1}{q}\left(\frac{\partial R_H}{\partial H}\right)^{-1}$$

On the basis of above equation, we could measure n_s values as 4.03×10^{10} cm^{-2} (2.52×10^{16} cm^{-3}) at 300 K. At 200 K, the n_s appeared to be an order of magnitude smaller than that at 300 K. From the fact that n_s is suppressed as the temperature (T) decreases as shown in Figure 3d, our MoS_2 sample exhibits a typical semiconducting behavior with a finite activation energy value. (After room temperature sheet resistance measurements, our Hall mobility could also be extracted out, to be ~200 cm^2/(V s), which is a few times lower than that of MESFET with NiO_x gate and it is attributed to the fact that our Hall sample cannot have the NiO_x gate which may help electron scattering reduction.)[46]

For our experiment, which was intended to clearly distinguish the properties between MISFET and MESFET, we fabricated 4L-MoS_2 MESFET with NiO_x (inset optical image in Figure 4a; W/L = 7.5/6 μm) and 4-layer MoS_2 MISFET with 50 nm-thin atomic layer deposited (ALD) Al_2O_3 top gate insulator (inset in Figure 4b; W/L = 10/5 μm), while those two devices were fabricated on separate glass substrates. (The layer thickness, 4-layer was confirmed by Raman spectroscopy and AFM topography

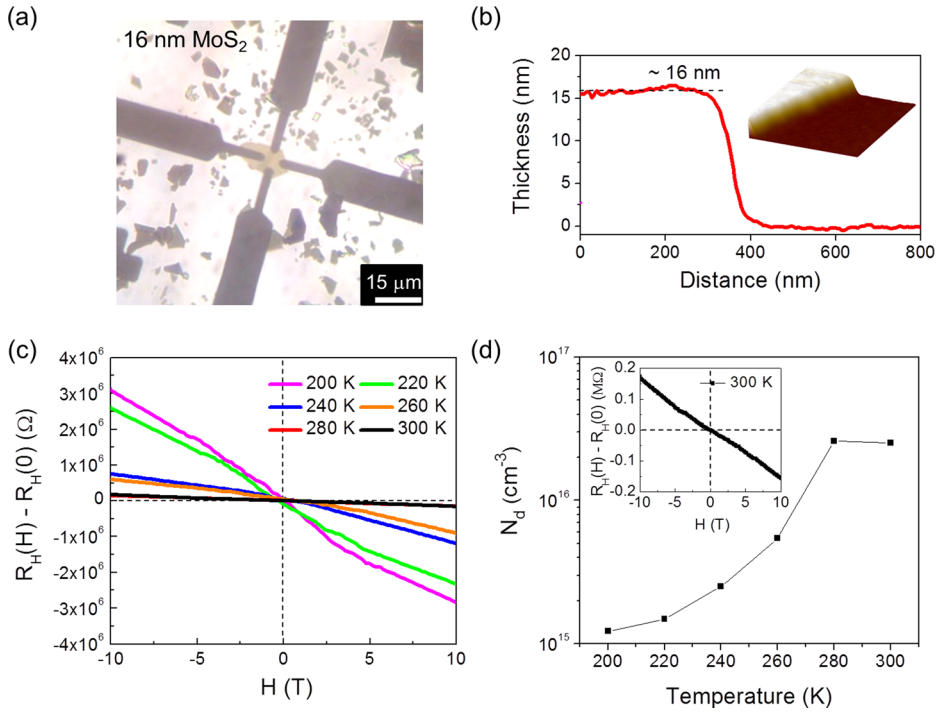

Figure 3. (a) The optical image and (b) thickness profile of 16 nm-thick MoS_2 sample for 4-probe Hall measurement. (c) Linear R_H variation under H sweep with various temperatures (T). (d) Plot of N_D *versus* temperature as achieved from the H sweep at different temperatures. The inset shows linear R_H variation under H sweep at 300 K.

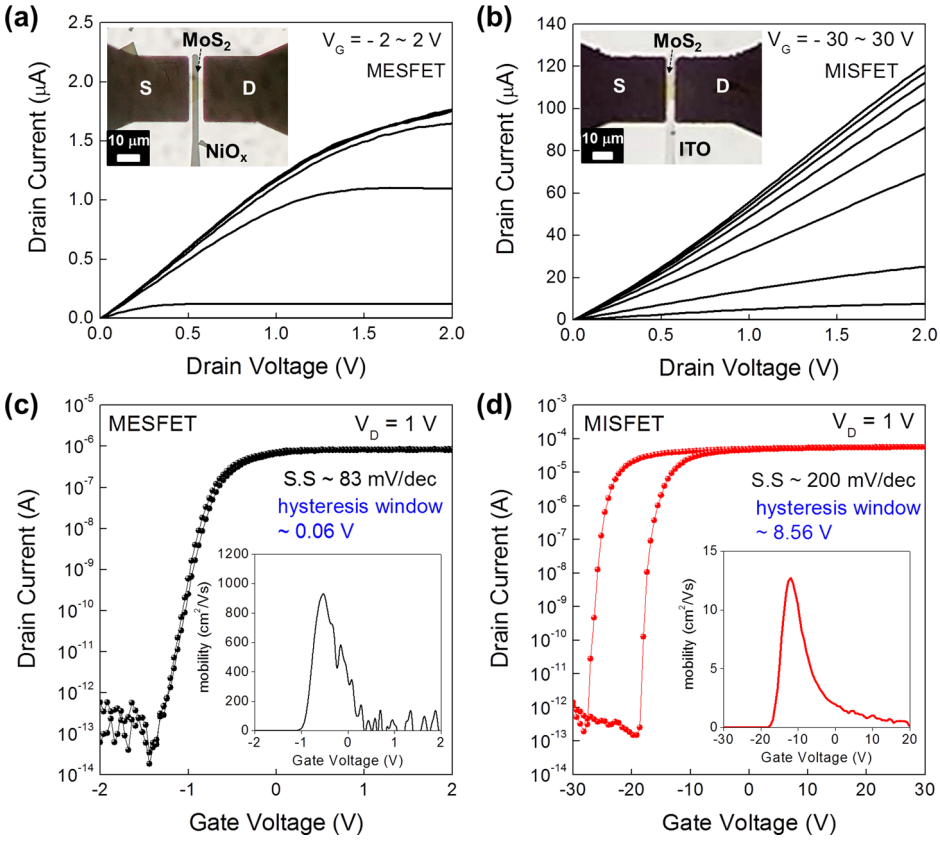

Figure 4. (a) Saturation I_D-V_{DS} behavior of our MESFET with 4L MoS_2. (b) Linear output behavior of MISFET with 4-layer MoS_2. (c) Transfer curves of our MESFET device show SS of only 83 mV/dec, 60 mV hysteresis window, on/off ratio of 1×10^7, and ~950 cm^2/V s for saturation mobility (inset). (d) Transfer curves of MISFET with ITO gate display 8.56 V hysteresis window, 200 mV SS, on/off ratio of 6×10^7, and its linear mobility of 12.5 cm^2/V s.

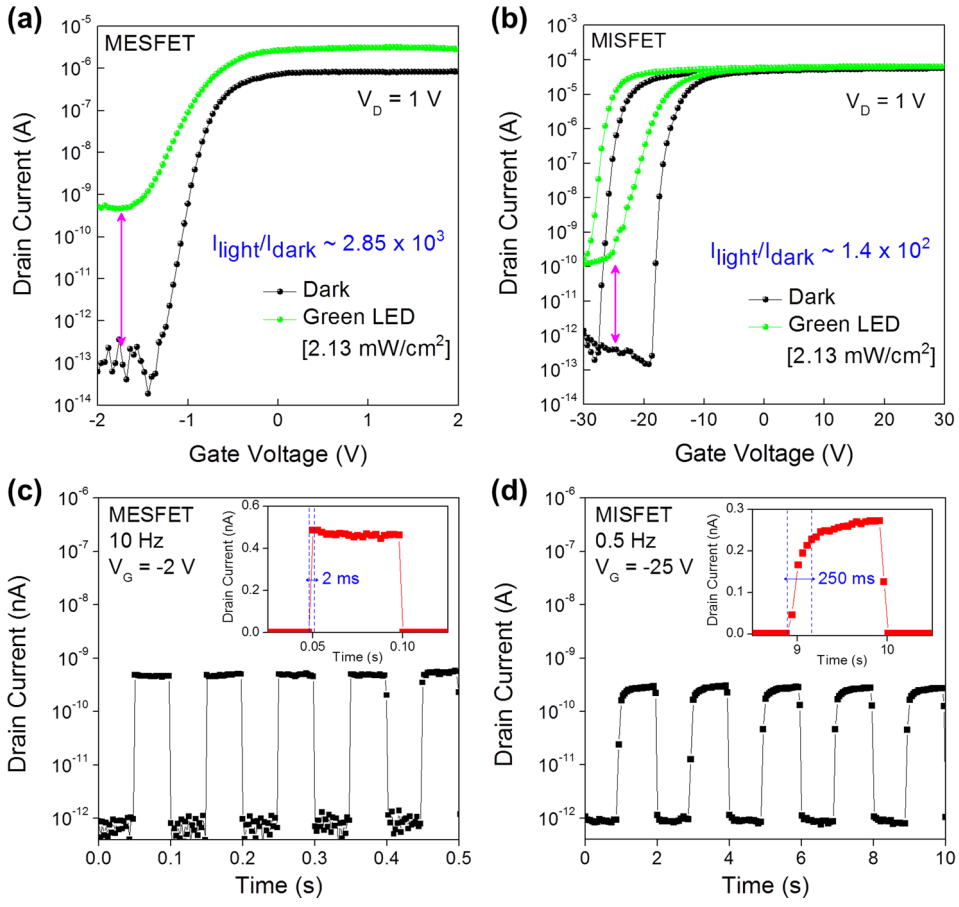

Figure 5. Photoinduced transfer curves of our (a) MESFET and (b) MISFET devices with transparent gate electrode, as obtained under green LED. Photo-to-dark ratio of MESFET (I_{light}/I_{dark}) appears an order of magnitude higher than that of MISFET device. Dynamic photoswitching behavior of our (c) MESFET and (d) MISFET devices; according to the respective insets, MESFET displays 2 orders of magnitude higher switching speed than MISFET along with slightly higher photocurrent.

in Supporting Information Figure S8.) According to the respective optical images, MESFET channel with semi-transparent NiO_x gate appears quite transparent on glass, while MISFET top-gate was covered by fully transparent indium–tin-oxide (ITO) electrode (back illumination was taken for photograph). Their respective output curves are shown in Figure 4, panels a and b, along with their inset device images for comparison; MESFET shows some saturation behavior unlike MISFET, which does appear almost completely linear. Such saturation behavior in MESFET with 4-layer MoS_2 comes from the easy channel-depletion (pinch-off) in drain side with V_{DS} increase which would cause even negative V_{GD}, while the on-state gate voltage of MISFET with the same 4-layer always provides the channel with charging-induced high density electron carriers to seldom cause such pinch-off in drain side channel. The transfer curves of the two devices are displayed in Figure 4c,d, where MISFET shows ~60 times higher drain current than MESFET under 1 V drain voltage. So, MISFET would be more advantageous in practical electronic applications requesting high current if reasonable threshold voltages are reproducibly controlled. However, according to the mobility plots in Figure 4d and its inset, the linear mobility of MISFET was limited to only ~12.5 cm^2/(V s) along with a large swing (SS = ~200 mV/dec), large hysteresis (8.56 V) and too much negative threshold voltages (~−20 V), while MESFET shows ~950 cm^2/(V s) as a saturation mobility, little hysteresis (0.06 V), and sharp swing (SS = 83 mV/dec) near −2 V (Figure 4c and inset). For the linear mobility (μ_{lin}) of MISFET with Al_2O_3 dielectric, conventional equation was used as $\mu_{lin} = (1/V_D C_{ox})(L/W)(\partial I_D/\partial V_G)$, where C_{ox} is the dielectric capacitance.[10] All the differences originate from the fact that the 4-layer channel of MISFET has two ~3 orders of magnitude higher carrier density (~10^{19} cm^{-3} or ~10^{12} cm^{-2}) drawn by gate charging,[25,26] which would however cause serious trap-induced interface scattering during operation. Moreover, we also suspect that ALD-process for high-k dielectric induces H atoms to MoS_2 channel by diffusion, and that the diffused H impurities play as scattering center.[47−49] Again, the high mobilities from our MESFETs are explained with the low densities of electron carrier and scattering center in the thin MoS_2 channel itself, while the MESFET operation also allows scattering-minimized transport without gate charging-induced interferences.[30,31]

Such a high intrinsic mobility in MoS_2 MESFET was supported by implementing phototransistor measurements, where 520 nm-wavelength green light emitting diode (LED) was used for light-detection performance comparison between the MISFET and MESFET (of Figure 5a,b). According to dynamic photoswitching behavior in Figure 5c,d (respectively with 10 and 0.5 Hz LED switching), the fast response time of 2 ms is obtained in MESFET with 4-layer MoS_2 at low gate voltages of −2 V, while more than 250 ms appears for 4-layer MoS_2 MISFET with ALD Al_2O_3 top-gate dielectric at high gate voltages of −25 V. Moreover, their respective phototo-dark I_D ratios are estimated to be 1.4×10^2 and 2.85×10^3 for MISFET and MESFET devices, which means MESFET photodetector is 100 times faster and 10 times more sensitive, although in fact 250 ms in our MoS_2 MISFET phototransistor is still quite good among many MoS_2 photo FET reports as summarized in Table 1.[50−53] We regard that the reason for the fast photoresponse is definitely related to 50−100 times higher mobility of MESFET than that of MISFET. (Responsivity of our MESFET under green LED was estimated to be 5000 and 1.1 A/W for ON and OFF states, respectively.)

As our final experimentation, we also attempted to demonstrate organic LED (OLED) switching using our MESFET. Despite the small I_D current of our MESFET, OLED switching was nicely operated by using the MESFET under low voltages ($V_{IN} = V_{DD} = 2$ V) (related circuits and demonstration details are found in Supporting Information Figure S9 and OLED operation video.avi file). This indicates that our MoS_2 nanosheet-based MESFET device is quite useful in electronics and optoelectronic applications, particularly for low voltage electronics.

TABLE 1. Summary Table of Dynamic Switching Properties and Photosensitivity Measured from MoS_2-Based Phototransistor in Air Ambient

	I_{light}/I_{dark} ratio	response time	light power	wavelength
Our MESFET	2.85×10^3	∼2 ms	2.13 mW/cm^2	520 nm
Our MISFET	1.4×10^2	∼250 ms	2.13 mW/cm^2	520 nm
ref47	$\sim 3 \times 10^2$	∼1 s	6 mW/cm^2	532 nm
ref48	$\sim 5 \times 10^2$	∼1 s	50 mW/cm^2	633 nm
ref49	Unknown	50 ms	80 μW	550 nm
ref50	∼30	4 s	4.25 μW	561 nm

CONCLUSION

In summary, we have fabricated MoS_2-based metal semiconductor field-effect transistors (MESFETs) with NiO_x Schottky electrode, where the maximum mobilities or carrier transport behavior of the Schottky devices may hardly be interfered by interface traps or an on-state gate field. Our MESFETs with 4−10 layer MoS_2 demonstrate high intrinsic-like mobilities of 500−1200 cm^2/(V s) at a certain low threshold voltage between −1 and −2 V with little gate bias-induced hysteresis, while they also exhibit very fast photoswitching in 2 ms playing as phototransistors with semitransparent NiO_x window. We conclude that our MESFET with van der Waals interface between NiO_x gate and MoS_2 channel would be a promising model nano FET with high speed, predictable low threshold voltage, and sharp swing behavior, to be applied for future nanoelectronics and nano-optoelectronics.

METHODS

Device Fabrication. All the MoS_2 nanosheets were mechanically exfoliated from bulk MoS_2 crystals (SPI supplies, natural molybdenite) and transferred to 285 nm SiO_2 grown on heavily doped p-type silicon substrate (285 nm-thick SiO_2/p^+-Si) or to glass substrate (Eagle 2000) by using a standard scotch tape method. For the source (S) and drain (D) ohmic contact electrodes Au/Ti (70/30 nm) were patterned (deposited at room temperature) on top of MoS_2 flakes by using photolithography, lift-off, and DC-sputter deposition processes. As the first layer, the Lift-Off-Layer (LOL: using a solution, LOL 2000, Micro Chemical) was coated, followed by thermal curing at 115 °C for 2 min. Then, photoresist (PR: SPR 3612, Micro Chemical) as the second layer was coated and baked at 95 °C for 2 min. The samples were exposed to UV light for 5 s under photomask aligner for S/D pattern. The samples were subsequently patterned with metal-ion-free (MIF) developer solution, and sequential DC-magnetron sputter-deposition of 30 nm-thin Ti and a 70 nm thin Au layers (Au/Ti) were carried out. For the liftoff process to finally define S/D electrode, acetone and LOL remover solvents were used. After that, the device was annealed at 250 °C with N_2 flow in rapid thermal annealing (RTA) system, to remove polymer residue and simultaneously to reduce contact resistance. A 150 nm-thick NiO_x Schottky contact gate electrode for MESFET (or Pt and Pd Schottky electrodes for diode) was patterned (deposited at room temperature) between the S/D electrodes by the same lithography and liftoff methods as performed for S/D contact, but for the deposition of NiO_x, we used the thermal evaporation of NiO_x powder while Pt and Pd films were deposited by DC-magnetron sputtering. The channel length, L of our MESFET was 6 μm and the gate length of NiO_x, Pt, and Pd was 3 μm in channel direction. NiO_x evaporation would hardly contaminate MoS_2 according to $I-V$ curves in Supporting Information Figure S10, which was achieved with and without NiO_x electrode on top of MoS_2.

Measurements and Characterizations. The thickness of MoS_2 flakes were first detected by optical microscope, then the exact layer number of each MoS_2 was characterized by AFM (XE-100, psia) and Raman spectroscopy. SEM was also necessary for the top view of our MESFET. All current−voltage ($I-V$) characteristics were measured by using a semiconductor parameter analyzer (HP 4155C, Agilent Technologies) in ambient air and room temperature. The Hall measurements for electron density determination of 23L-thin MoS_2 on glass were implemented at various temperatures in the range of 200−300 K by applying AC current of 0.4 Hz and 0.1 mA as input signal frequency and amplitude, respectively, under the magnetic field (H) sweep from −10 to 10 T. We used the physical property measurement system (PPMS) for Hall measurements. Photoinduced static and dynamic signals were measured by using 520 nm-wavelength green LED (2.13 mW/cm^2), which was pulsed in square wave for the dynamic photoswitching by pulse generator (AFG3022B, Tektronix). For the OLED operation, we used the conventional OLED devices (Courtesy from Samsung Display Co.).

Conflict of Interest: The authors declare no competing financial interest.

Supporting Information Available: Optical images of several MoS_2 nanosheets which play as the channel of MESFET, schematic energy ban diagram, schematic illustrations for MESFET operations, comparison between NiO_x and pure metal contact for MESFET, transconductance plots of 10-layer MoS_2 MESFET, Padovani−Stratton parameter for electron density estimation, reproducibility of MESFET, AFM profile and Raman spectra obtained from 4-layer MoS_2, OLED operation using our MESFET. The Supporting Information is available free of charge on the ACS Publications website at DOI: 10.1021/acsnano.5b02785.

Acknowledgment. The authors acknowledge the financial support from NRF (NRL program: Grant No. 2014R1A2A1A0-1004815), Nano-Materials Technology Development Program (Grant No. 2012M3A7B4034985), NRF of Korea (Grant No. 2011-0018306), KISTI supercomputing center (Project No. KSC-2013-C3-008) and Brain Korea 21 plus Program.

REFERENCES AND NOTES

1. Coleman, J. N.; Lotya, M.; O'Neill, A.; Bergin, S. D.; King, P. J.; Khan, U.; Young, K.; Gaucher, A.; De, S.; Smith, R. J. et al. Two-Dimensional Nanosheets Produced by Liquid Exfoliation of Layered Materials. *Science* **2011**, *331*, 568–571.
2. Chhowalla, M.; Shin, H. S.; Eda, G.; Li, L.- J.; Loh, K. P.; Zhang, H. The Chemistry of Two-Dimensional Layered Transition Metal Dichalcogenide Nanosheets. *Nat. Chem.* **2013**, *5*, 263–275.
3. Radisavljevic, B.; Whitwick, M. B.; Kis, A. Integrated Circuits and Logic Operations Based on Single-Layer MoS_2. *ACS Nano* **2011**, *5*, 9934–9938.
4. Yu, L.; Lee, Y.-H.; Ling, X.; Santos, E. J. G.; Shin, Y. C.; Lin, Y.; Dubey, M.; Kaxiras, E.; Kong, J.; Wang, H.; et al. Graphene/MoS_2 Hybrid Technology for Large-Scale Two-Dimensional Electronics. *Nano Lett.* **2014**, *14*, 3055–3063.
5. Cheng, R.; Jiang, S.; Chen, Y.; Liu, Y.; Weiss, N.; Cheng, H.-C.; Wu, H.; Huang, Y.; Duan, X. Few-Layer Molybdenum Disulfide Transistors and Circuits for High-Speed Flexible Electronics. *Nat. Commun.* **2014**, *5*, 5143.
6. Roy, T.; Tosun, M.; Kang, J. S.; Sachid, A. B.; Desai, S. B.; Hettick, M.; Hu, C. C.; Javey, A. Field-Effect Transistors Built from All Two-Dimensional Material Components. *ACS Nano* **2014**, *8*, 6259–6264.
7. Wang, Q. H.; Kourosh, K. Z.; Kis, A.; Coleman, J. N.; Strano, M. S. Electronics and Optoelectronics of Two-Dimensional Transition Metal Dichalcogenides. *Nat. Nanotechnol.* **2012**, *7*, 699–712.
8. Lee, H. S.; Min, S. W.; Chang, Y. G.; Park, M. K.; Nam, T.; Kim, H.; Kim, J. H.; Ryu, S.; Im, S. MoS_2 Nanosheet Phototransistors with Thickness-Modulated Optical Energy Gap. *Nano Lett.* **2012**, *12*, 3695–3700.
9. Kim, S.; Konar, A.; Hwang, W. S.; Lee, J. H.; Lee, J.; Yang, J.; Jung, C.; Kim, H.; Yoo, J. B.; Choi, J. Y.; et al. High-Mobility and Low-Power Thin-Film Transistors Based on Multilayer MoS_2 Crystals. *Nat. Commun.* **2012**, *3*, 1011.
10. Radisavljevic, B.; Radenovic, A.; Brivio, J.; Giacometti, V.; Kis, A. Single-Layer MoS_2 Transistors. *Nat. Nanotechnol.* **2011**, *6*, 147–150.
11. Liu, H.; Ye, P. D. MoS_2 Dual-Gate MOSFET with Atomic-Layer-Deposited Al_2O_3 as Top-Gate Dielectric. *IEEE Electron Device Lett.* **2012**, *33*, 546–548.
12. Chuang, H.-J.; Tan, X.; Ghimire, N. J.; Perera, M. M.; Chamlagain, B.; Cheng, M. M.-C.; Yan, J.; Mandrus, D.; Tománek, D.; Zhou, Z. High Mobility WSe_2 p- and n-Type Field-Effect Transistors Contacted by Highly Doped Graphene for Low-Resistance Contacts. *Nano Lett.* **2014**, *14*, 3594–3601.
13. Fang, H.; Tosun, M.; Seol, G.; Chang, T. C.; Takei, K.; Guo, J.; Javey, A. Degenerate n-Doping of Few-Layer Transition Metal Dichalcogenides by Potassium. *Nano Lett.* **2013**, *13*, 1991–1995.
14. Fang, H.; Chuang, S.; Chang, T. C.; Takei, K.; Takahashi, T.; Javey, A. High-Performance Single Layered WSe_2 p-FETs with Chemically Doped Contacts. *Nano Lett.* **2012**, *12*, 3788–3792.
15. Pospischil, A.; Furchi, M. M.; Mueller, T. Solar-Energy Conversion and Light Emission in an Atomic Monolayer p-n Diode. *Nat. Nanotechnol.* **2014**, *9*, 257–261.
16. Baugher, B. W. H.; Churchill, H. O. H.; Yang, Y.; Jarillo-Herrero, P. Optoelectronic Devices Based on Electrically Tunable p-n Diodes in A Monolayer Dichalcogenide. *Nat. Nanotechnol.* **2014**, *9*, 262–267.
17. Ross, J. S.; Klement, P.; Jones, A. M.; Ghimire, N. J.; Yan, J.; Mandrus, D. G.; Taniguchi, T.; Watanabe, K.; Kitamura, K.; Yao, W.; et al. Electrically Tunable Excitonic Light-Emitting Diodes Based on Monolayer WSe_2 p-n Junctions. *Nat. Nanotechnol.* **2014**, *9*, 268–272.
18. Pradhan, N. R.; Rhodes, D.; Xin, Y.; Memaran, S.; Bhaskaran, L.; Siddiq, M.; Hill, S.; Ajayan, P. M.; Balicas, L. Ambipolar Molybdenum Diselenide Field-Effect Transistors: Field-Effect and Hall Mobilities. *ACS Nano* **2014**, *8*, 7923–7929.
19. Lin, Y. F.; Xu, Y.; Wang, S. T.; Li, S. L.; Yamamoto, M.; Ferreira, A. A.; Li, W.; Sun, H.; Nakaharai, S.; Jian, W. B.; et al. Ambipolar $MoTe_2$ Transistors and Their Applications in Logic Circuits. *Adv. Mater.* **2014**, *26*, 3263–3269.
20. Cui, X.; Lee, G. H.; Kim, Y. D.; Arefe, G.; Huang, P. Y.; Lee, C. H.; Chenet, D. A.; Zhang, X.; Wang, L.; Ye, F.; et al. Multi-Terminal Transport Measurements of MoS_2 Using a van der Waals Heterostructure Device Platform. *Nat. Nanotechnol.* **2015**, *10*, 534–540.
21. Lee, G. H.; Yu, Y. J.; Cui, X.; Petrone, N.; Lee, C. H.; Choi, M. S.; Lee, D. Y.; Lee, C.; Yoo, W. J.; et al. Flexible and Transparent MoS_2 Field-Effect Transistors on Hexagonal Boron Nitride-Graphene Heterostructures. *ACS Nano* **2013**, *7*, 7931–7936.
22. Chen, X.; Wu, Z.; Xu, S.; Wang, L.; Huang, R.; Han, Y.; Ye, W.; Xiong, W.; Han, T.; Long, G.; et al. Probing The Electron States and Metal-Insulator Transition Mechanisms in Molybdenum Disulphide Vertical Heterostructures. *Nat. Commun.* **2015**, *6*, 6088.
23. Muller, R. S.; Kamin, T. I.; Chan, M. *Device Electronics for Integrated Circuits*, 3rd ed.; Zobrist, B., Ed.; John Wiley & Sons, , New York, 2003; Ch. 8.
24. Zou, X.; Wang, J.; Chiu, C. H.; Wu, Y.; Xiao, X.; Jiang, C.; Wu, W. W.; Mai, L.; Chen, T.; Li, J.; et al. Interface Engineering for High-Performance Top-Gated MoS_2 Field-Effect Transistors. *Adv. Mater.* **2014**, *26*, 6255–6261.
25. Radisavljevic, B.; Kis, A. Mobility Engineering and A Metal-Insulator Transition in Monolayer MoS_2. *Nat. Mater.* **2013**, *12*, 815–820.
26. Baugher, B. W. H.; Churchill, H. O. H.; Yang, Y.; Jarillo-Herrero, P. Intrinsic Electronic Transport Properties of High-Quality Monolayer and Bilayer MoS_2. *Nano Lett.* **2013**, *13*, 4212–4216.
27. Min, S. W.; Lee, H. S.; Choi, H. J.; Park, M. K.; Nam, T.; Kim, H.; Ryu, S.; Im, S. Nanosheet Thickness-Modulated MoS_2 Dielectric Property Evidenced by Field-Effect Transistor Performance. *Nanoscale* **2013**, *5*, 548–551.
28. Na, J.; Joo, M.; Shin, M.; Huh, J.; Kim, J.; Piao, M.; Jin, J.; Choi, H. J.; Shin, J. H.; et al. Low-Frequency Noise in Multilayer MoS_2 Field-Effect Transistors: the Effect of High-k Passivation. *Nanoscale* **2014**, *6*, 433–441.
29. Ma, R. M.; Dai, L.; Qin, G. G. High-Performance Nano-Schottky Diodes and Nano-MESFETs Made on Single CdS Nanobelts. *Nano Lett.* **2007**, *7*, 868–873.
30. Frenzel, H.; Lajn, A.; von Wenckstern, H.; Lorenz, M.; Schein, F.; Zhang, Z.; Grundmann, M. Recent Progress on ZnO-Based Metal-Semiconductor Field-Effect Transistors and Their Application in Transparent Integrated Circuits. *Adv. Mater.* **2010**, *22*, 5332–5349.
31. Khan, T.; Vasileska, D.; Thornton, T. J. Subthreshold Electron Mobility in SOI MOSFETs and MESFETs. *IEEE Trans. Electron Devices* **2005**, *52*, 1622–1626.
32. Lee, H. S.; Lee, K. H.; Chang, Y. G.; Raza, S. R. A.; Im, S.; Kim, D. H.; Kim, H. R.; Lee, G. H. Photogating and Electrical-Gating of Amorphous GaSnZnO-Based Inverter with

Light-Transmitting Gate Electrode. *Appl. Phys. Lett.* **2011**, *98*, 223505.
33. Lee, K.; Kim, J. H.; Im, S. Probing the Work Function of A Gate Metal with A Top-Gate ZnO-Thin-Film Transistor with A Polymer Dielectric. *Appl. Phys. Lett.* **2006**, *88*, 023504.
34. Padovani, F. A.; Stratton, R. Field and Thermionic-Field Emission in Schottky Barriers. *Solid-State Electron.* **1966**, *9*, 695–707.
35. Chuang, S.; Kapadia, R.; Fang, H.; Chang, T. C.; Yen, W. C.; Chueh, Y. L.; Javey, A. Near-Ideal Electric Properties of InAs/WSe_2 van der Waals Heterojunction Diodes. *Appl. Phys. Lett.* **2013**, *102*, 242101.
36. Allen, M. J.; Tung, V. C.; Kaner, R. B. Honeycomb Carbon: A Review of Graphene. *Chem. Rev.* **2010**, *110*, 132–145.
37. Leonard, F.; Talin, A. A. Electrical Contacts to One- and Two-Dimensional Nanomaterials. *Nat. Nanotechnol.* **2011**, *6*, 773–783.
38. Sze, S. M. *Physics of Semiconductor Devices*, 2nd ed.; John Wiley & Sons: New York, 1981; Ch. 7.
39. Muller, R. S.; Kamin, T. I.; Chan, M. *Device Electronics for Integrated Circuits*, 3rd ed.; Zobrist, B., Ed.; John Wiley & Sons: New York, 2003; Ch. 4.
40. El-Mahalawy, S. H.; Evans, B. L. Temperature Dependence of The Electrical Conductivity and Hall Coefficient in 2H-MoS_2, $MoSe_2$, WSe_2, and $MoTe_2$. *Phys. Status Solidi B* **1977**, *79*, 713–722.
41. Fivaz, R.; Mooser, E. Mobility of Charge Carriers in Semiconducting Layer Structures. *Phys. Rev.* **1967**, *163*, 743–755.
42. Grant, A. J.; Griffiths, T. M.; Pitt, G. D.; Yoffe, A. D. The Electrical Properties and The Magnitude of The Indirect Gap in The Semiconducting Transition Metal Dichalcogenide Layer Crystals. *J. Phys. C: Solid State Phys.* **1975**, *8*, L17–L23.
43. Lee, K.; Kim, H. Y.; Lotya, M.; Coleman, J. N.; Kim, G. T.; Duesberg, G. S. Electrical Characteristics of Molybdenum Disulfide Flakes Produced by Liquid Exfoliation. *Adv. Mater.* **2011**, *23*, 4178–4182.
44. Sze, S. M. *Physics of Semiconductor Devices*, 3rd ed.; John Wiley & Sons: New York, 1981; Ch. 1.
45. Zhang, Y.; Ye, J.; Matsuhashi, Y.; Iwasa, Y. Ambipolar MoS_2 Thin Flake Transistors. *Nano Lett.* **2012**, *12*, 1136–1140.
46. Jena, D.; Konar, A. Enhancement of Carrier Mobility in Semiconductor Nanostructures by Dielectric Engineering. *Phys. Rev. Lett.* **2007**, *98*, 136805.
47. Ryu, B.; Lee, Y. T.; Lee, K. H.; Ha, R.; Park, J. H.; Choi, H. J.; Im, S. Photostable Dynamic Rectification of One-Dimensional Schottky Diode Circuits with a ZnO Nanowire Doped by H During Passivation. *Nano Lett.* **2011**, *11*, 4246–4250.
48. Late, D. J.; Liu, B.; Matte, H. S. S. R.; Dravid, V. P.; Rao, C. N. R. Hysteresis in Single-Layer MoS_2 Field Effect Transistors. *ACS Nano* **2012**, *6*, 5635–5641.
49. Choi, K.; Raza, S. R. A.; Lee, H. S.; Jeon, P. J.; Pezeshki, A.; Min, S. W.; Kim, J. S.; Yoon, W.; Ju, S. Y.; Lee, K.; et al. Trap Density Probing on Top-Gate MoS_2 Nanosheet Field-Effect Transistors by Photo-Excited Charge Collection Spectroscopy. *Nanoscale* **2015**, *7*, 5617–5623.
50. Kwon, J.; Hong, Y. K.; Han, G.; Omkaram, I.; Choi, W.; Kim, S.; Yoon, Y. Giant Photoamplification in Indirect-Bandgap Multilayer MoS_2 Phototransistors with Local Bottom-Gate Structures. *Adv. Mater.* **2015**, *27*, 2126–2230.
51. Choi, W.; Cho, M. Y.; Konar, A.; Lee, J. H.; Cha, G. B.; Hong, S. C.; Kim, S.; Kim, J.; Jena, D.; Joo, J.; et al. High-Detectivity Multilayer MoS_2 Phototransistors with Spectral Response from Ultraviolet to Infrared. *Adv. Mater.* **2012**, *24*, 5832–5836.
52. Yin, Z. Y.; Li, H.; Li, H.; Jiang, L.; Shi, Y.; Sun, Y.; Lu, G.; Zhang, Q.; Chen, X.; Zhang, H. Single-Layer MoS_2 Phototransistors. *ACS Nano* **2012**, *6*, 74–80.
53. Lopez-Sanchez, O.; Lembke, D.; Kayci, M.; Redenovic, A.; Kis, A. Ultrasensitive Photodetectors Based On Monolayer MoS_2. *Nat. Nanotechnol.* **2013**, *8*, 497–501.